### Title
Experimental evaluation of shear connectors using reactive powder concrete under natural curing condition




### Authors
He, Shaohua
Mosallam, Ayman S
Fang, Zhi
et al.



### Publication Date
2018-12-01

### DOI
10.1016/j.conbuildmat.2018.10.063

Peer reviewed

Construction and Building Materials 191 (2018) 775–786

Contents lists available at ScienceDirect

Construction and Building Materials

journal homepage: www.elsevier.com/locate/conbuildmat

# Experimental evaluation of shear connectors using reactive powder concrete under natural curing condition

Shaohua He [a], Ayman S. Mosallam [b], Zhi Fang [c,*], Xiaolong Sun [a], Jie Su [c]

[a] School of Civil and Transportation Engineering, Guangdong University of Technology, Guangzhou, Guangdong 510006, China
[b] Department of Civil and Environmental Engineering, University of California, Irvine, CA 92697, USA
[c] College of Civil Engineering, Hunan University, Changsha, Hunan 410082, China

## HIGHLIGHTS

- The performance of shear connectors embedded in RPC is evaluated by push-out tests.
- Load-strain responses for the shear connectors using RPC under push-out load are discussed.
- The shrinkage effect of RPC material on performance of shear connectors is analyzed.
- The applicability of existing predicting equations to PBL using RPC with shrinkage effect is assessed.

## ARTICLE INFO

*Article history:*
Received 23 June 2018
Received in revised form 16 September 2018
Accepted 8 October 2018
Available online 16 October 2018

*Keywords:*
Push-out test
PBL
RPC
Shrinkage
CFSC
Steel stud

## ABSTRACT

In hybrid girder bridges, an efficient type of steel-concrete joint, the so called concrete filled steel cells (CFSCs), can be used to transfer forces between the steel and concrete girders. In the CFSCs, where shear connectors embedded in the concrete core, the bearing capacity of shear connectors is significantly affected by the side confinement effects of steel cells. Shrinkage of concrete may change the interfacial restraints from the steel cells. So far, the influence of concrete shrinkage on the behavior of shear connectors in CFSCs has not been deeply addressed. This paper presents an experimental study of the structural response of shear connectors using reactive powder concrete (RPC) encased in CFSCs. To determine the shrinkage effects of RPC, results from two series of experimental programs are discussed: the first series included testing of twelve plug-in type push-out specimens to assess the performance of perfobond strip (PBL) connectors. The second series consists of testing two plug-in type push-out specimens and eight CFSC type push-out specimens to evaluate the behavior of PBL and steel stud connectors. Results indicated that initial cracks due to shrinkage were observed at the steel cell/RPC interface, which was very detrimental to connectors' stiffness and strengths. Comparing to connectors with exposed RPC, the average ultimate bond strength at the CFSC steel cell/RPC interface dropped by 15%. Results also indicated that failure of steel stud and transverse steel rebar was barely influenced by RPC shrinkage. Furthermore, a comparison between experimental and predicting results was conducted to assess the applicability of the existing analytical models in predicting the behavior of PBL embedded in RPC with shrinkage.



## 1. Introduction

Steel-concrete hybrid girders, in which steel girders and concrete girders are integrally connected via steel-concrete joints and deform as a single unit, have gained popularity in the construction of large-span bridges. For a steel-concrete hybrid girder bridge, the steel-concrete joint connecting steel and concrete girders in different spans is considered to be the key component. The joint structure should provide adequate strength to transfer forces between different members and to prevent local failure prior to other parts of the girder. To date, several types of steel-concrete joint have been developed and adopted in constructed hybrid girder bridges. One practical form of such joints is in the form of concrete filled steel cells (CFSCs) (see Fig. 1). As shown in the figure, steel cells filled with concrete are distributed along the lateral direction of the cross-section, and force transmission in CFSCs is primary relied on shear connectors between the steel cell and concrete core.

* Corresponding author.
*E-mail address:* fangzhi@hnu.edu.cn (Z. Fang).

https://doi.org/10.1016/j.conbuildmat.2018.10.063
0950-0618/

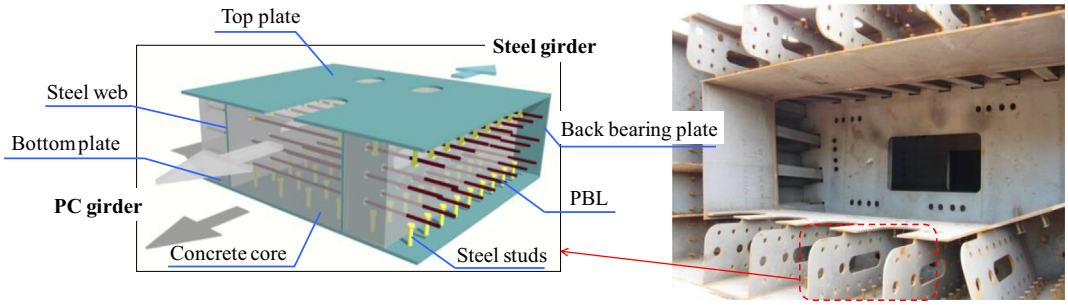


**Fig. 1.** Schematic View of Typical CFSC in a Steel-Concrete Joint.

Both steel stud and perfobond strip (PBL) shear connectors are widely used in CFSCs. Steel stud is a type of traditional shear connector that can be automatically welded and produced in a large scale. A significant number of studies have been conducted on the performance of steel studs through experimental and numerical methods, and design formulas for steel studs in steel/concrete composite structures also have been included in current codes [1–3]. The PBL connector, consisting of a perforated steel plate and a transverse steel rebar passing through the holes, was first introduced in 1987 [4]. The shear resistance of PBL mainly comes from bonding effects at the steel plate/concrete interface, concrete dowel action, and resistance of transverse steel rebar. Since the PBL was proposed, structural behavior including the failure mechanism, ultimate strength, and load-slip relationship have been gradually investigated by many researchers [5–18]. Previous study indicated that the bearing capacity of a steel stud or PBL shear connector is determined by the mechanical properties of concrete surrounding the connector, in addition to the geometrical dimensions and strength of steel elements.

Mechanical property of concrete grout, which filled into steel cells, plays an essential role in achieving favorable performance of shear connectors in CFSCs. In previously established hybrid girder bridges, the steel-concrete joint is commonly filled with normal concrete. There are many disadvantages of using normal concrete in CFSCs applications that include: (i) the problem arising from shrinkage of normal concrete at the steel cells causing separation between steel and concrete, and decreasing the safety and durability of such joints [19]; (ii) the problems associated with coarse aggregates and the high density of steel reinforcements in the CFSCs, leading to difficulties in achieving the desired concrete quality that is poured into the cells; (iii) the limitation in bridge's spanning capacity due to the low strength of normal concrete at the joint zones [20]. To prevent such problems, reactive powder concrete (*RPC*) has been introduced to replace normal concrete in steel-concrete joints recently. The ultra-high strength of RPC can improve the load carrying capacity of the joint [21], thus, spanning capacity of hybrid girder bridges could be improved when RPC is used. Another benefit of using RPC is the absence of coarse aggregates resulting in the ease of placing concrete at the joint zone limited space. In addition, the small shrinkage of RPC under hot steam curing could also lead to better bond state between joint steel components and concrete. With such excellent merits, RPC has been utilized in the construction of the steel-concrete joint of the Nujiang Bridge [21], the Jiayu Yangtze River Bridge, and the Shishou Yangtze River Bridge in China.

Although RPC has been applied in bridge engineering practices, only few research studies have been performed to validate and assess the mechanical performance of shear connectors encased in CFSCs with RPC. Previous studies indicated that the shrinkage of RPC under natural maintains cannot be ignored, showing an average ultimate shrinkage strain of approximately 600–800$\mu\varepsilon$, which is about twice as much of that when hot steam curing is used [22]. In engineering practice, hot steam curing is usually impractical for RPC filled into steel-concrete joint due to site limitations. For this reason, initial cracking may develop at the steel/-concrete interface when RPC is utilized. Additionally, the interfacial restrains at the steel plate/concrete interface is beneficial in enhancing the shear capacity of PBL [23–26]. However, the shrinkage of RPC may decrease the confinement effects from the steel cells and results in a drop of PBL resistance. As such, it is crucial to evaluate the shrinkage effects of RPC on the performance of the shear connectors in CFSC to achieve reliable and sustainable design.

This study presents a description and results of a series of experiments that was performed to assess the structural behavior of shear connectors using RPC in steel-concrete joints in the absence of hot steam curing. Some significance contributions of this research are the pioneering study of the impact of shrinkage on the behavior of shear connectors fabricated using RPC. The Nujiang Bridge in China was selected as the base for this study. Two plug-in type and eight CFSC type push-out specimens were evaluated. Experimental results including failure modes, ultimate resistance, slip capacity, load-slip behavior, and load-strain responses of the connectors using RPC were obtained and presented. By comparing experimental results of both the current and a previous study performed by authors [21], the effects of RPC shrinkage on behavior of the shear connectors using RPC were analyzed. In order to examine the feasibility of existing formulas for PBL with exposed concrete to that encased in CFSCs of steel-concrete joints, a comparison between the present and previous experimental results and available equations for PBL connectors in the literature is presented. Finally, an analytical equation for the capacity prediction of PBL in CFSCs fabricated using RPC under natural treatment is proposed.

## 2. Experimental program

### 2.1. Push-out test specimens

A total of ten push-out specimens, including two plug-in type and eight CFSC type of specimens were fabricated and tested. The configurations of the push-out specimens are illustrated in Fig. 2. The bottom surface of steel plates in all specimens of the plug-in type was covered with an air gap to eliminate the influence of local direct contact mechanism, and all CFSC specimens were fabricated with an air layer at the bottom of core concrete to exclude the local direct contacting effect. The geometric configurations of push-out specimens were established in accordance with those used by He et al. [23]. Typical dimensions and details of the plug-in type and the CFSC specimens are presented in Figs. 3 and 4, respectively.

The main objective of the test program is to evaluate the performance of shear connector using RPC and ascertain the effects of RPC shrinkage on behavior of the connectors. Variables such as presence of shear connectors and the test arrangement are evaluated. Table 1 summarizes the parameters of all the specimens. The

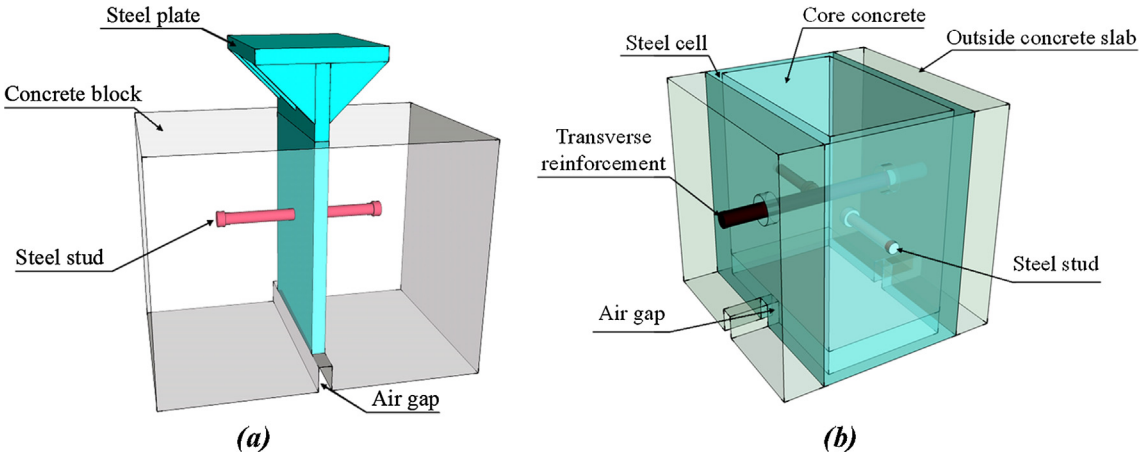


**Fig. 2.** Structural Layout of Push-Out Specimens: (a) Schematics of Plug-In Specimen Layout; (b) Schematics of CFSC Specimen Layout.

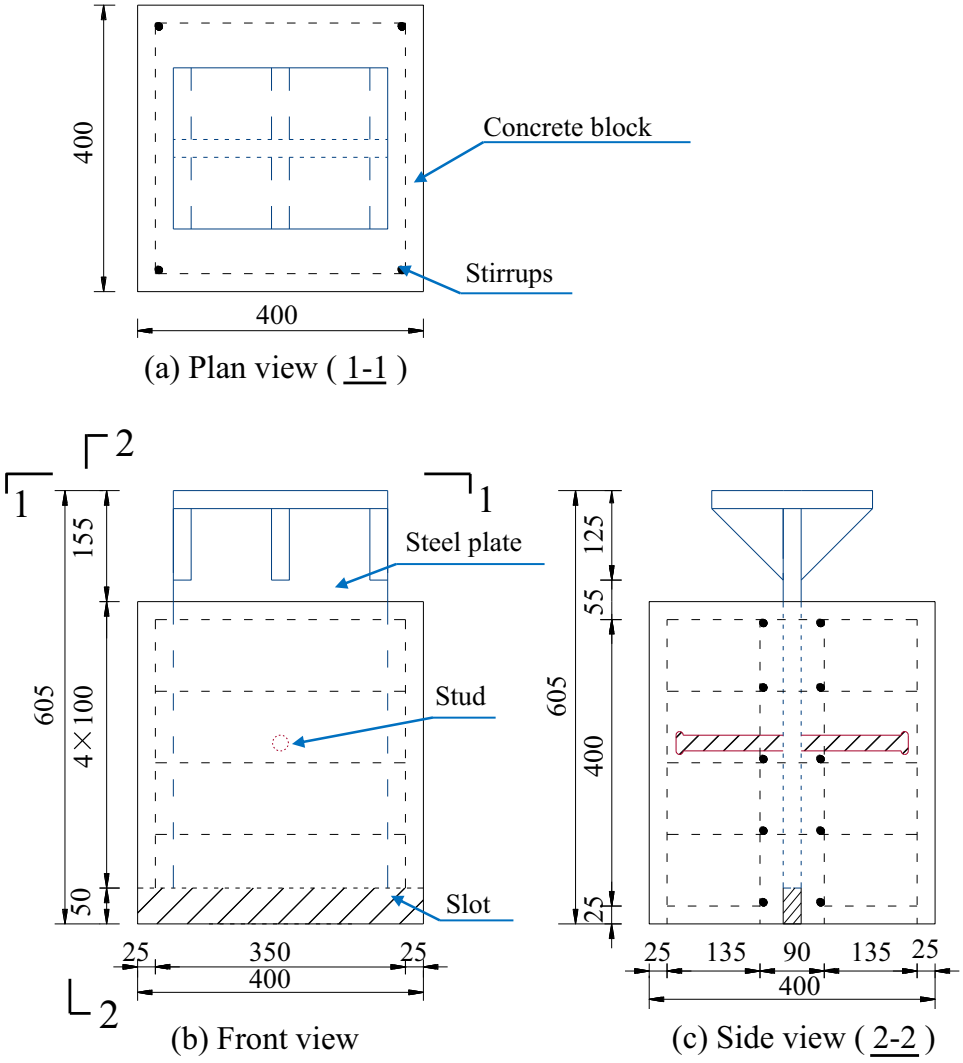


**Fig. 3.** Geometry of the Plug-in Type Push-out Specimens (*unit: mm*).

first character "P" or "C" in the specimen label denotes the specimen of plug-in type and CFSC type, respectively; the second designation "R" represent the push-out specimen fabricated using Reactive Powder Concrete (*RPC*); The character "b", "s", and "p" represent the interface bond at the steel plate/concrete contact surface, steel stud, and PBL, respectively; the number 1 or 0 after the "b", "s", or "p" indicates whether the corresponding part exists. For example, "CR-b1s0p1" indicates a CFSC type of push-out specimen fabricated using RPC with the steel/concrete interface bond and the PBL connector but without the steel studs.

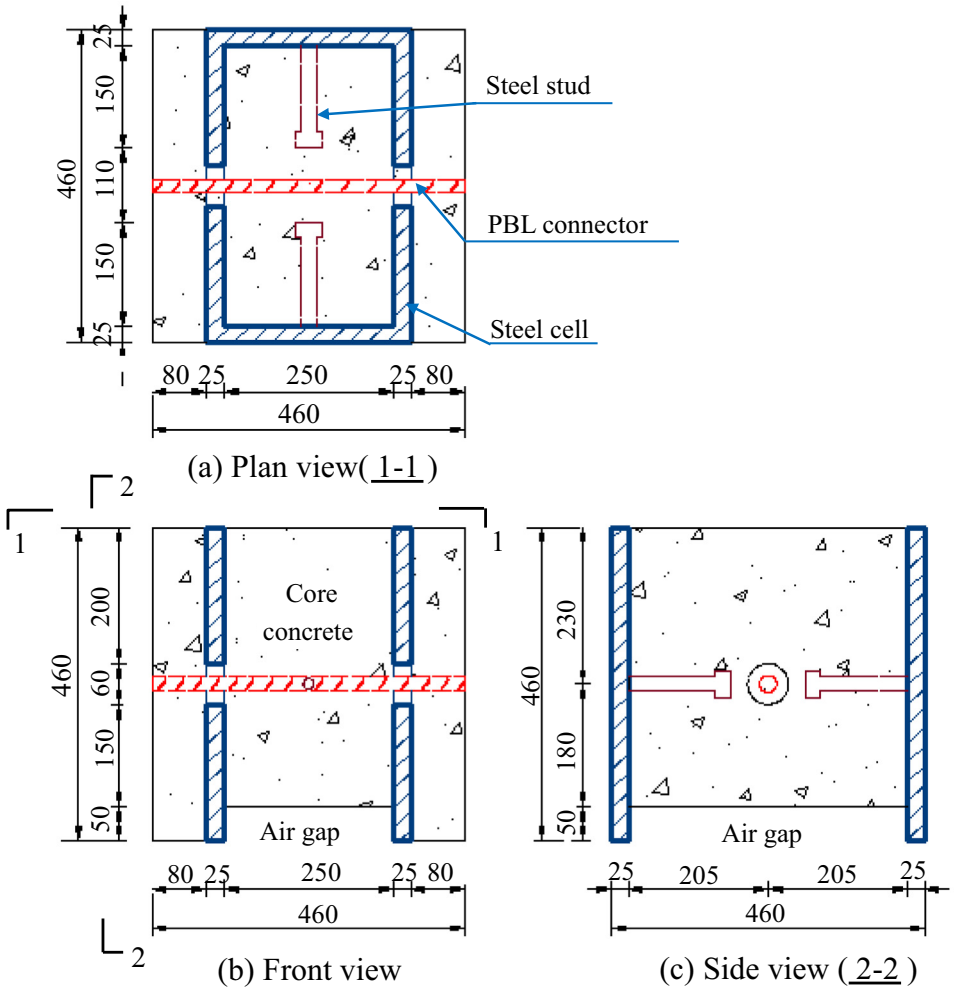


**Fig. 4.** Geometry of the CFSC Type Push-out Specimens (Group *CR-b1s1p1 example, unit: mm*).

**Table 1**
Specimen Characteristics.

| Group No. | Specimen code | State | Connector types | | Dimensions of PBL (mm) | | Dimensions of stud (mm) | Transverse rebar grade |
|---|---|---|---|---|---|---|---|---|
| | | | PBL | Stud | Rebar diameter | Hole diameter | | |
| 1 | PR-b1s1p0 | With interface bond and steel studs | | √ | – | 60 | 22 × 150 | – |
| 2 | CR-b1s0p0 | With interface bond | | | – | 60 | – | – |
| 3 | CR-b1s1p0 | With interface bond and steel studs | | √ | – | 60 | 22 × 150 | – |
| 4 | CR-b1s0p1 | With interface bond and PBL | √ | | 20 | 60 | – | HRB335 |
| 5 | CR-b1s1p1 | With interface bond, studs, and PBL | √ | √ | 20 | 60 | 22 × 150 | HRB335 |

*2.2. Materials properties*

The RPC used in this study is composed of ordinary Portland cement, silica fume, quartz sand, ground quartz, and water reducer. The mix proportions are shown in Table 2. The average particle size of silica fume was 0.70 $\mu m$. The maximum particle size of quartz sand and ground quartz were 0.60 mm and 45.0 $\mu m$ gradation, respectively. Six standard cubes with side length of 100.0 mm were cast in preparation for the RPC average compressive strength determinations and cured alongside the push-out specimens. Eighteen 100.0 mm × 100.0 mm × 300.0 mm prisms were fabricated from the same patch and were tested to measure the prismatic strength, elasticity modulus and shrinkage. The material properties of the RPC used in all specimens were as follows: design strength 100.0 MPa, 28-day compressive strength 115.5 MPa, prismatic strength 92.6 MPa, and Young's modulus 42.6 GPa. The shrinkage of the RPC material measured at the day of push-out load applied was 619 $\mu\varepsilon$.

Structural steel (grade Q345C) with nominal yield strength of 345.0 MPa and a thickness of 25.0 mm was used in all specimens. HPB235 steel reinforcement bars (*with nominal yield strength of 235.0 MPa*) were adopted as the reinforcements in

**Table 2**
RPC Mix Design (*Relative weight ratios to cement*).

| Cement | Silica fume | Quartz sand | Ground quartz | Water reducer | Water |
|---|---|---|---|---|---|
| 1.0 | 0.25 | 1.1 | 0.1 | 0.025 | 0.275 |

concrete blocks of the plug-in type specimens. Steel rebars of HRB335 (*with nominal yield stress of 335.0 MPa*) were used for the transverse rebar of the PBL. Headed studs with a diameter of 22.0 mm and a length of 150.0 mm, which selected based on Chinese Code [27], were used in the tests programs. Table 3 summarizes the characteristics of the steel materials, where $f_y$ is the yield strength, $f_u$ is the ultimate tensile strength, $E_s$ is the modulus of elasticity, and $\delta$ is the percentage elongation.

### 2.3. Test Setup and instrumentation

Figs. 5 and 6 show the test setup for the specimens in plug-in type and CFSC type, respectively. To record the relative slip between steel plate and concrete block, two linear variable differential transducers (LVDTs) were installed on the two opposite sides of the push-out specimens. A steel block with cross-sectional sizes of 230.0 mm × 200.0 mm × 50.0 mm (width × length × thickness) was placed on the top of CFSC specimens for load application. For specimens with steel studs (i.e. groups PR-b1s1p0, CR-b1s1p0 and CR-b1s1p1), electronic strain gauges were mounted on steel studs to evaluate their stress state. For specimens with PBL connectors (i.e. groups CR-b1s0p1 and CR-b1s1p1), strain gauges were installed on the transverse steel rebar to monitor strain variation.

The structural behavior of shear connectors was evaluated using the push-out test specified in Eurocode 4 [1]. All tests were performed in a calibrated 5000.0 kN capacity testing machine. Prior to reaching specimens' ultimate capacity, the push-out tests followed a force-control regime with a constant rate of 5.0 kN/s. As the load approaches its ultimate value, a displacement-control regime with a constant rate of 0.3 mm/min was employed. Loading continued until the relative displacement reached to approximately 30.0 mm.

## 3. Test results and discussion

### 3.1. General observations

Push-out tests were performed to assess the ultimate resistance, slip capacity, load-slip relationship, and load-strain responses of the connectors following the analysis method developed in previous studies [21,23]. Table 4 summarizes the peak load, $V_u$, and the associated relative slip $S_u$. For the ease of compar-

**Table 3**
Mechanical Properties of Steel Reinforcements.

| Material type | Steel grade | Diameter $d$(mm) | Average $f_y$ (MPa) | Average $f_u$ (MPa) | Average $E_s$ (GPa) | $\delta$(%) |
|---|---|---|---|---|---|---|
| Reinforcements | HPB235 | 10 | 298 | 446 | 201 | 25 |
| | HRB335 | 20 | 358 | 529 | 207 | 26 |
| Stud | – | 22 | 383 | 478 | – | 17 |

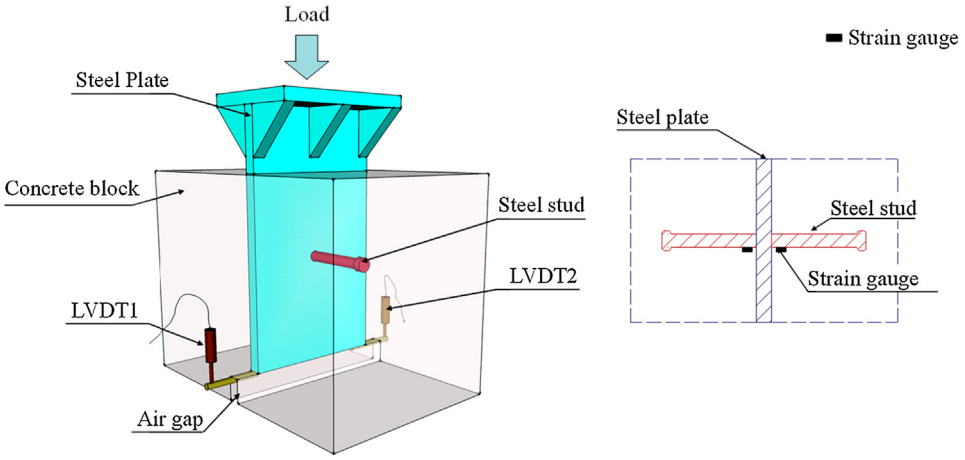


**Fig. 5.** Setup for Plug-in Type Push-Out Tests.

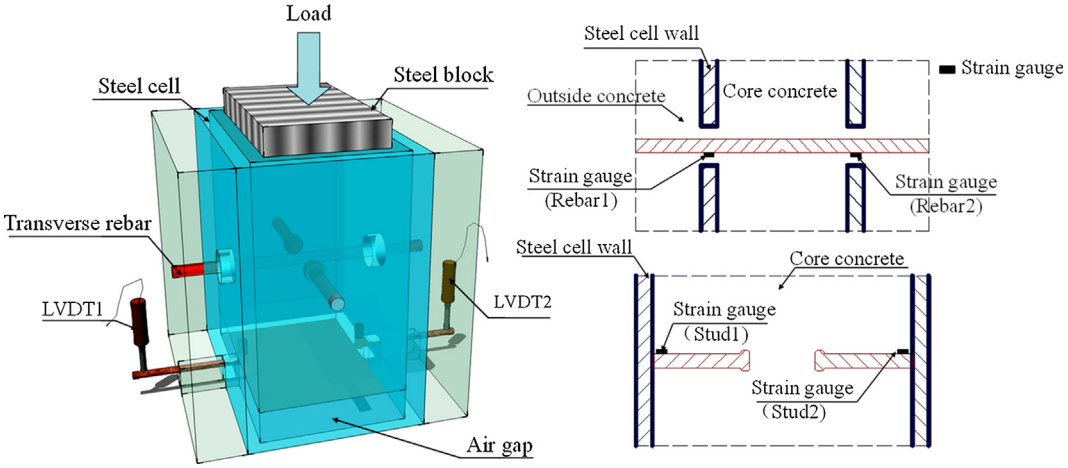


**Fig. 6.** Setup for CFSC Type Push-Out Tests.

**Table 4**
Experimental Results of Specimens Subjected to Push-Out Loads.

| | Group NO. | Specimen code | Peak load, $V_u$ (kN) | | | Relative slip at $V_u$, $S_u$ (mm) | | | Failure modes |
|---|---|---|---|---|---|---|---|---|---|
| | | | Spec.-1 | Spec.-2 | Ave. | Spec.-1 | Spec.-2 | Ave. | |
| Previous tests [21] | 1 | PR-b1r0d0 | 360 | 342 | 351 | 0.53 | 0.60 | 0.57 | Shear failure at the interface |
| | 2 | PR-b1r1d1 | 651 | 683 | 667 | 16.34 | 20.02 | 18.18 | Fracture of the PBL |
| Current tests | 3 | PR-b1s1p0 | 552 | 521 | 537 | 6.34 | 6.92 | 6.63 | Shear failure of steel studs |
| | 4 | CR-b1s0p0 | 558 | 520 | 539 | 4.89 | 5.07 | 4.98 | Shear failure at the interface |
| | 5 | CR-b1s1p0 | 730 | 693 | 712 | 7.23 | 6.35 | 6.79 | Shear failure of steel studs |
| | 6 | CR-b1s0p1 | 887 | 959 | 923 | 16.6 | 15.77 | 16.19 | Fracture of the PBL |
| | 7 | CR-b1s1p1 | 1238 | 1039 | 1139 | 16.9 | 17.98 | 17.44 | Fracture of shear connectors |

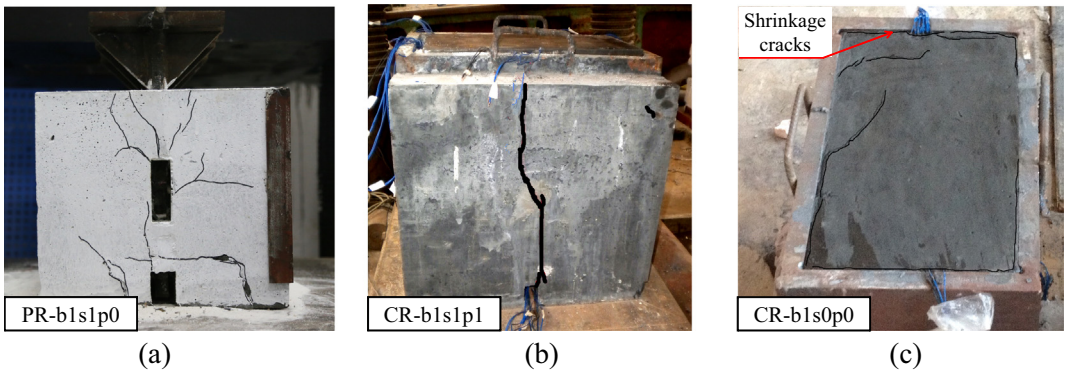


**Fig. 7.** Crack Distribution and Propagation in Different Specimens: *(a) Group PR-b1s1p0; (b) Group CR-b1s1p1; (c) Group CR-b1s0p0.*

ison and discussion, test results for the pure bond specimens of group PR-b1r0d0 (with interfacial bond between the steel plate and concrete only), and the bonded PBL specimens of group PR-b1r1d1 (with interfacial bond and reinforced concrete dowel) that were previously reported by He et al. [21] are also presented in Table 4. For groups PR-b1r0d0 and PR-b1r1d1, the characters "*PR*", and the number 1 or 0, have same meaning to those of group PR-b1s1p0 in the current tests program. The characters "b", "r", and "d" represent the interfacial bond at the steel plate/concrete contact surface, the transverse steel rebar and the concrete dowel, respectively. As shown in Table 4, the differences between the experimental results for the two identical specimens in each group are small. This proved the validity of the test results.

Fig. 7 shows the typical crack development in the different push-out specimens. As shown in the figure, for plug-in type specimen PR-b1s1p0, several cracks were developed at the side surfaces of the concrete blocks with increasing applied load. For CFSC type specimens, with a reinforced concrete dowel passing through the holes in the steel cell walls (e.g. specimens CR-b1s0p1 and CR-b1s1p1), only few small vertical cracks appeared on the outside concrete slabs surface. It should be emphasized that due to the shrinkage of RPC material, initial cracks around almost the entire perimeter of steel cell were observed for all CFSC specimens before load application. Fig. 7(c) shows the typical shrinkage cracks that were developed in group CR-b1s0p0. The initial cracks resulted from RPC shrinkage reduced the ultimate strength of the connectors considerably as it will be explained later in this paper.

Ultimate failure of the plug-in type push-out specimens occurred when the steel plate was pushed out from the concrete block and the steel studs were fractured from welding roots. The failure mode of the CFSC type push-out specimens was in the form of concrete core detachment from the steel cell and the fracture of the shear connectors at the contact surface between the steel cell and concrete. All steel components were removed from concrete after testing to examine the state of the steel members. No buckling was found in the steel plates and steel cells for all tests, except for the local scratches that appeared on the steel plate surface around the welding roots of steel studs. As it was observed previously [5–9], the transverse steel rebar of PBL connector failed in a tension shear mode. The ultimate failure modes of the steel studs and the transverse rebars are show in Fig. 8.

### 3.2. Load-slip curves

Fig. 9 shows the load-slip curves for all push-out specimens evaluated in this study. In this figure, an average curve of two identical specimens from each group is plotted. In order to assess the shrinkage effects on behavior of the connectors, previously published load-slip curves for the bonded PBL plug-in type specimens of group PR-b1r1d1 [21] are presented in Fig. 9.

The plug-in type of specimen PR-b1s1p0 consists of two steel studs embedded in exposed RPC blocks. The load-slip curves for group PR-b1s1p0 are plotted in Fig. 9(a). From this figure, one can see that the behavior pattern of the connector consists of: (i) an *initial elastic stage* with a slip less than 1.0 mm, (ii) a *yield-hardening stage* with a slip between 1.0 mm and 7.0 mm, and (iii) a *post-failure stage* that occurs at larger slip values. In the initial elastic stage, slip linearly increased until the load approached to approximately 75% of the ultimate value. As the interfacial bond at the steel plate/concrete interface gradually deteriorated, steel studs yielded and load-slip curves behaved nonlinearly up to the peak load. Once the steel studs sheared off at the peak loads, a sudden strength degradation is observed that was followed by a stable plateau at large slips.

Fig. 9(b) shows the load-slip curves for the CFSC type of the pure bond specimens of group CR-b1s0p0. The specimens of this group were evaluated in order to assess the behavior of the interfacial bond between the steel cell and the encased RPC core. As the load linearly increased to approximately 50% of the peak load, the load-slip curves of this group exhibited a significant nonlinear hard-

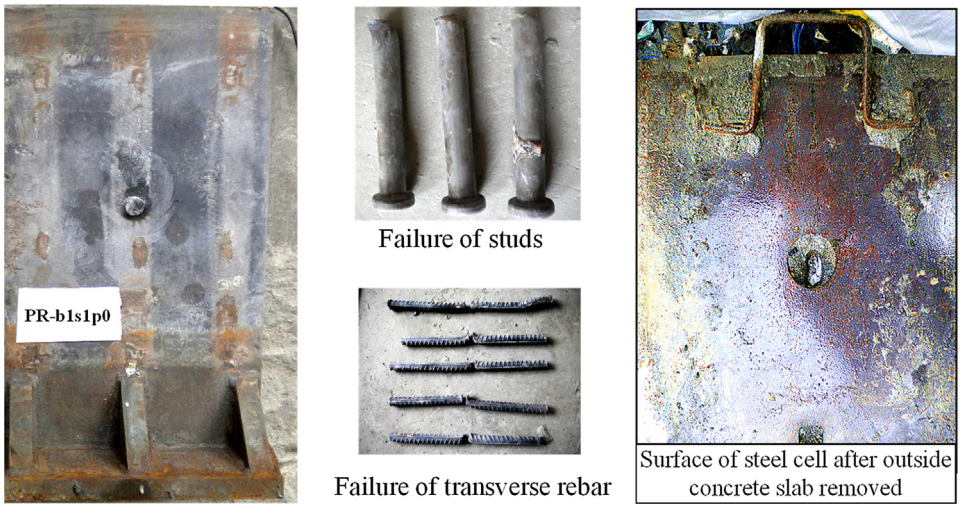


**Fig. 8.** Failure Modes of the Steel Components.

ening phase, as shown in Fig. 9(b). The peak load was attained at a relative slip of about 4.98 mm, while a sharp load drop was observed once failure was initiated. Afterwards, a nearly constant residual load, due to friction, of 350.0 kN was maintained up the maximum recorded relative slip value of 29.4 mm. The interfacial bond stresses developed between the steel cell and RPC core at the ultimate and residual loads were 1.0 MPa and 0.68 MPa, respectively.

Fig. 9(c) shows the load-slip curves for the specimens of group CR-b1s1p0. These specimens were designed and evaluated in order to assess the performance of the steel studs in encased RPC. As shown in this figure, in the elastic stage, the relative slip increased linearly as the load increased. The steel studs yielded at a load of about 55% of the peak loads, after which the behavior became non-linear up to the fractures the studs. The connectors' peak load was achieved at a relative slip of approximately 6.8 mm. As compared to the pure bond specimen of group CR-b1s0p0, providing two steel studs inside the RPC core of specimens CR-b1s1p0 led to a 32% increase in the connector ultimate strength and a relative slip increase up to 36%. As shown in Fig. 9(c), a larger residual resistance was maintained for CR-b1s1p0 after failure in comparison with that of CR-b1s0p0. This may be explained by the fact that the fracture of sections of the steel studs provided higher mechanical interlocking effects as compared to that of the pure bond specimens of group CR-b1s0p0.

Fig. 9(d) presents the load-slip curves for the CFSC type of PBL specimens in group CR-b1s0p1. The specimens of this group were

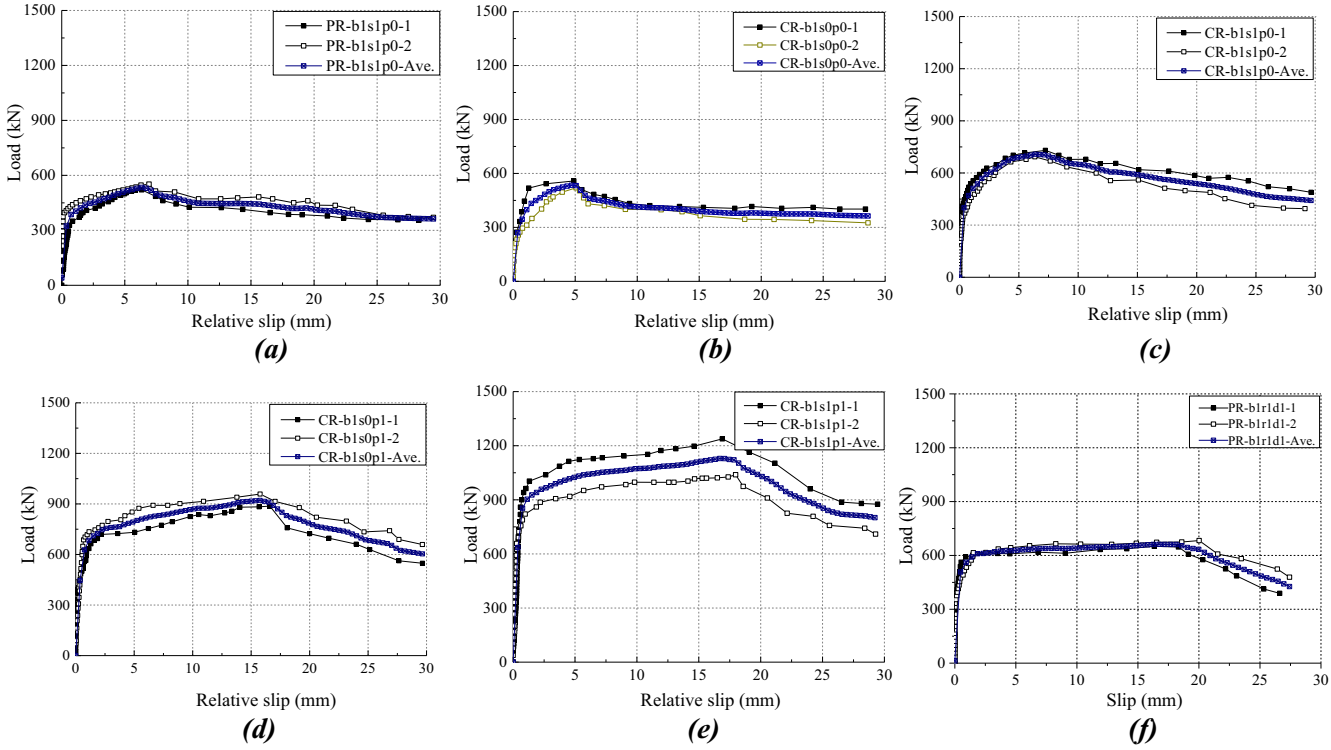


**Fig. 9.** Load-Slip Curves for CFSC Specimens: (a) Group PR-b1s1p0; (b) Group CR-b1s0p0; (c) Group CR-b1s1p0; (d) Group CR-b1s0p1; (e) Group CR-b1s1p1; (f) Group PR-b1r1d1.

designed to explore the behavior of PBL encased in RPC. As shown in this figure, yield occurred to the transverse steel rebar at a load of approximately 75% of the ultimate loads. Also, a significant yield-hardening phase was observed prior to the achievement of peak load. The transverse rebars fractured at an average relative slip of 16.19 mm, which is obviously larger than the corresponding value obtained from CR-b1s1p0 tests. This can be attributed to the deformability of the transverse steel rebar, that failed in a tension/shear failure mode in group CR-b1s0p1, is relatively larger than the deformability observed for the case of specimens CR-b1s1p0, where pure shear was the dominated failure mode of the steel studs. Due to the detachment of the RPC core from the steel cell that resulted from shrinkage, considerable discrepancies was observed between the load-slip curves obtained for the two identical specimens of CR-b1s0p1.

Fig. 9(e) presents the load-slip curves for the CFSC type specimens of group CR-b1s1p1. This type of specimens was evaluated to assess the combined action of steel studs and PBL encased in RPC. As shown in this figure, at the beginning of loading procedure, a slight relative slip occurred between the steel cell and concrete in group CR-b1s1p1. At moderate loading level, the connector behavior was linear up to approximately 70–80% of their peak loads. Beyond this load level, nonlinear behavior was observed up to the failure of the connectors. Thereafter, a progressive load decrease towards a slip was followed in their post-peak load stage. The small fluctuations in load-slip curves after yielding of the connectors for specimen CR-b1s1p1 imply the fracture of the steel studs.

For the convenience of discussion, the load-slip curves of the bonded PBL specimens with exposed RPC in group PR-b1r1d1 that were previously published by authors [21] are shown in Fig. 9(f). In the ultimate range, the load-slip curves behaved nearly bilinear. Each curve consists of a linear segment up to approximately 80–90% of the peak load, and a non-linear pattern up to failure that continued to the post-peak phase. The post-peak resistance is primarily caused by the interfacial friction between the steel plate and the concrete. The average ultimate load and relative slip of PR-b1r1d1 were 667.0 kN and 18.18 mm, respectively.

### 3.3. Load-strain curves

In order to explore the stress state of the shear connectors, the strain results for both the steel studs and transverse steel rebars of PBL obtained from the present and previous tests [21] are shown in Fig. 10. The positive and negative strains in the figure represent tension and compression strains, respectively.

Fig. 10(a) shows the load-strain relationships for the steel studs of groups PR-b1s1p0 and CR-b1s1p0. As shown in this figure, nearly identical strain values were measured by strain gauges located at the steel stud's shank, near the welding root, for specimens PR-b1s1p0 and CR-b1s1p0. It should be noted that the contact area between the steel cell and the RPC core of specimen CR-b1s1p0 is 1.8 times of that of PR-b1s1p0 specimen; however, one can see from these curves that yield load of specimen CR-b1s1p0 is less than that of PR-b1s1p0 specimen. This is clearly due to the early damage of chemical adhesion at the steel cell/RPC core interface in CR-b1s1p0 resulted from RPC shrinkage. The similar ultimate strains of the studs from the two types of test arrangements demonstrated that the failure of steel studs was varied hardly with the shrinkage of RPC.

Fig. 10(b) shows the load-strain relationships for the transverse steel rebars of groups PR-b1r1d1 and CR-b1s0p1. It shows that the shrinkage of RPC seems to have no noticeable adverse effect on the ultimate strain of the steel rebars, which is consistent with the similar transverse rebar failure modes in different push-out test arrangements. In the linear part of the curves, little strain was recorded for the transverse rebars prior to reaching a load of 260.0 kN, thereafter mechanism of the PBL was activated and strains in transverse rebar rapidly increased up to the failure. Although visible discreteness was observed between the load-strain curves from the identical gauges of "rebar1" and "rebar2", the ultimate strains for the rebars obtained from the two strain gauges were close with an average value of 2400 $\mu\varepsilon$, which similar to the case observed for the transverse rebars of PBL reported earlier [9].

Fig. 10(c) presents the load-strain relationships for both the steel studs and transverse steel rebars of specimen CR-b1s1p1. As shown in this figure, at low load level, very low strain values were recorded for the steel studs and rebars, indicating that the load transferred from the RPC core to the steel cell through the bonding action along the steel/concrete interface. The activation of the connector mechanisms is initiated once failure occurred to the bondline. As the load approached to approximately 25% of the peak load, strains in both the steel studs and rebars increased simultaneously. Analyzing steel studs strain results indicates that, the studs deactivated at a strain level of approximately 1200 $\mu\varepsilon$. The transverse steel rebars failed at an average ultimate strain of around 2300$\mu\varepsilon$. The similar increasing trend of the load-strain curves of the steel studs and rebars indicates that the two types of connectors were activated once the chemical adhesion between the steel and concrete was damaged.

### 3.4. Influence of RPC shrinkage effects

The RPC shrinkage is generally caused by the loss of water, hydration of cement and carbonation. There are several types of

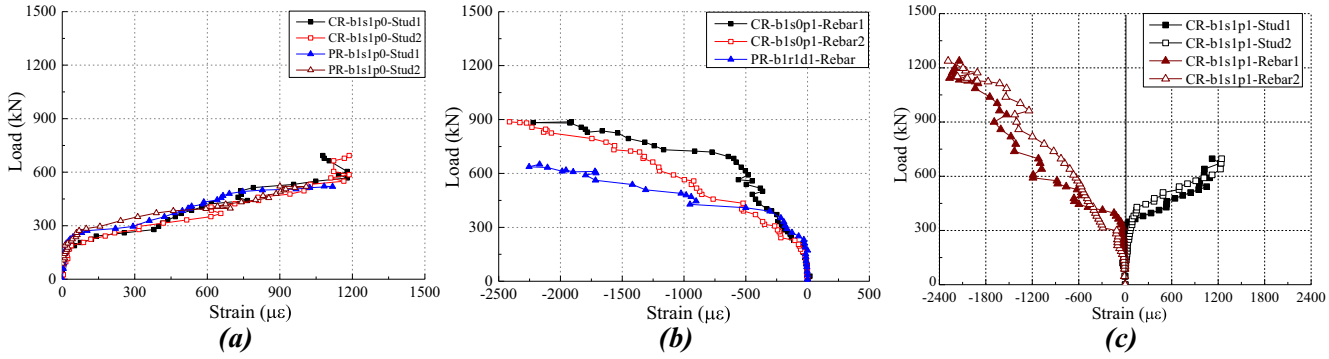


**Fig. 10.** Load-Strain Curves for CFSC Specimens: (a) Specimens of Groups CR-b1s1p0 and PR-b1s1p0; (b) Specimens in Groups CR-b1s0p1 and PR-b1r1d1; (c) Specimens in Group CR-b1s1p1.

shrinkage, in which drying shrinkage and autogenous shrinkage are the dominated ones. Due to the high cement content and low water to cement ratio of the RPC material, the total shrinkage of RPC is comparatively large as compared to that of normal concrete [28]. For the current tests, the damage associated with the shrinkage for the push-out specimens was in the form of surface cracking of the RPC material and the detachment of the RPC core from the steel cell. Due to concrete exposure, damage resulted from RPC shrinkage is insignificant for the plug-in type push-out specimens. The detachment of the RPC core from the steel cell may be attributed to the shrinkage of the restrained RPC inside the steel cells in CFSC specimens. For this reason, the effect of RPC shrinkage was analyzed via a comparison between experimental results obtained from the plug-in type specimens (e.g. groups PR-b1r0d0, PR-b1r1d1 and PR-b1s1p0) and the CFSC type specimens (e.g. groups CR-b1s0p0, CR-b1s0p1 and CR-b1s1p0).

From Table 4, one can see that the ultimate load obtained from the pure bond specimens of group CR-b1s0p0 is 1.5 times of that of PR-b1r0d0, despite the fact that the steel/concrete contact area of specimen CR-b1s0p0 is 1.8 times larger than that of PR-b1r0d0 specimens. The effects of RPC shrinkage decreased the average ultimate bonding stress at the steel cell/concrete interface of CR-b1s0p0 specimens by 15%, as compared to that of the PR-b1r0d0 specimens with exposed RPC. Additionally, the relative slip at specimen CR-b1s0p0 ultimate load significantly improved by the shrinkage effects, showing a relative slip increment of 7.7 times the corresponding value obtained from specimen PR-b1r0d0. A possible explanation for this augmentation may be ascribed to the fact that the ultimate resistance for PR-b1r0d0 was primarily provided by the chemical adhesion, while the ultimate resistance of specimen CR-b1s0p0 results from micro-interlocking and friction that were only activated when relative slip grows large.

The effect of RPC shrinkage on the performance of shear connectors was investigated using the plug-in type and the CFSC type of specimens with steel studs or PBLs. As shown in Table 4, the ultimate load of specimens with two steel studs that are embedded in the restrained RPC core of group CR-b1s1p0 is 1.3 times the ultimate resistance of PR-b1s1p0 specimen with exposed RPC. However, the relative slip values obtained from the two specimens groups are almost identical. Also, the ultimate load of specimen CR-b1s0p1 with restrained RPC core is 1.4 times of that for PR-b1r1d1 with exposed RPC, and the relative slip obtained from group CR-b1s0p1 decreased by 11% in comparison with that of the PR-b1r1d1. It is necessary to emphasize that the connectors' ultimate strength measured from the push-out tests consists of two parts: (i) the shear mechanisms of the connectors, and (ii) the bonding actions at the steel/concrete contact surface. The nominal shear strength $\sigma_{nor.}$ introduced herein in order to evaluate the influence of RPC shrinkage and its effect on connectors performance. The nominal shear strength, $\sigma_{nor.}$, is defined as the ultimate load, $V_u$, of a specimen divided by the steel/concrete contacting area $A_{sc}$, thus:

$$\sigma_{nor.} = V_u/A_{sc} \quad (1)$$

With the help of Eq. (1), the $\sigma_{nor.}$ for push-out specimens with the exposed and restrained RPC, respectively, are computed and summarized in Fig. 11. As shown in Fig. 11, the $\sigma_{nor.}$ of group CR-b1s1p0 is 74% as much that of PR-b1s1p0, and the $\sigma_{nor.}$ of group CR-b1s0p1 is 77% as much that of PR-b1r1d1. There are a number of factors that might have caused such a reduction in the shear resistance of the specimens. Among these is the possibility that shrinkage of the RPC material may has caused large decrease in steel/concrete interfacial bond strength. The relatively large difference in experimental results obtained from the plug-in type and the CFSC type indicates that the connectors' push-out resistance is sensitive to the shrinkage of the RPC materials as well as the condition of the steel-concrete interface.

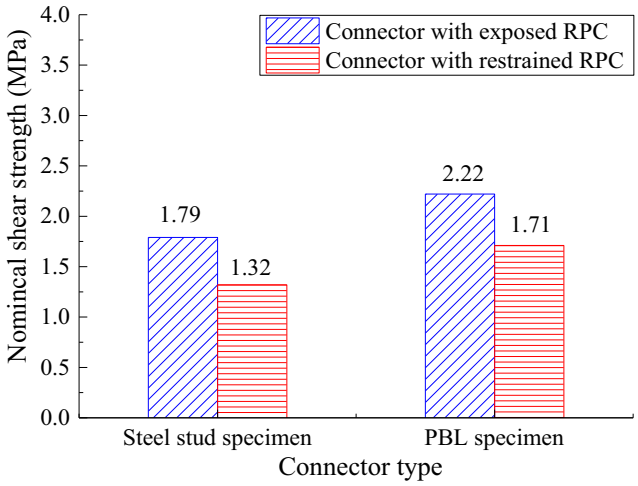


**Fig. 11.** Comparisons between $\sigma_{nor.}$ for Connectors Embedded in Exposed and Restrained RPC.

## 4. Equations for predicting the PBL capacity

### 4.1. Evaluation of existing analytical models

Based on the literature review, there is no equation in current design codes that determine the ultimate resistance of the PBL embedded in restrained RPC that considers the shrinkage effects. However, there are a number of equations for predicting shear capacity of PBL using conventional concrete. In order to assess the applicability of the existing equations to the PBL embedded in restrained RPC in steel-concrete joints, experimental results obtained from the present and previous tests and predicted results generated using typical equations are compared. Table 5 presents several typical equations that are commonly used to predict shear strength of PBL connectors.

Although expressions summarized in Table 5 are based on push-out experimental results of specimens fabricated with conventional concrete, lightweight concrete and ultra-high performance concrete (UHPC), these equations are used to compare its results with ultimate PBL strengths obtained from current experiments. The ultimate shear strength was computed for the PBL specimens in plug-in type (PR-b1r1d1) and CFSC type (CR-b1s0p1). Table 6 shows the ratios of predicted ultimate shear resistance to experimentally obtained ultimate strength of PBL. From this table, one can see that the equations listed in Table 5 for predicting ultimate resistance of PBL produced poor correlation with the experiments for all specimens, except for Eq. (7). The equations provided by Hans-Peter [13], Vianna et al. [11], Su et al. [5],and Wang et al. [8] overestimated the experimental strength of PR-b1r1d1, while the equation developed by JSCE [12] and Zheng et al. [6] resulted in a conservative strength results.

Eq. (2) provided unsafe ultimate resistance prediction for PR-b1r1d1 and conservative results for CR-b1s0p1, which may be attributed to the fact that this equation was developed based on experimental results obtained from PBL with conventional concrete and steel plates yielding failure mode. Obviously, they are very different from the present design and observed failure modes. In addition, the bonding action at the steel/concrete interface was not included in this expression.

Eqs. (3–2) and (8) overestimated the ultimate strength of all specimens. Eq. (3–2) considered the contribution of concrete local

**Table 5**
Equations to Predict Connector's Ultimate Shear Resistance.

| References | Equation | | Unit |
|---|---|---|---|
| Hans-Peter et al. [13] | $V_u = 2.257D^2 f_c$ | (2) | Force: N Length: mm Strength: MPa |
| Vianna et al. [11] | *For* $f_{ck} \le 30MPa$ $q_u = 152.9 + 3.21 \times 10^{-3}(h_{sc}t_{sc}f_{ck}) - 0.86 \times 10^{-3}A_{sc}\sqrt{f_{ck}}$ | (3–1) | |
| | *For* $f_{ck} > 30MPa$ $q_u = 31.8 + 1.9 \times 10^{-3}(h_{sc}t_{sc}f_{ck}) + 0.53 \times 10^{-6}(A_{tr}f_y) - 0.6 \times 10^{-6}A_{sc}\sqrt{f_{ck}}$ | (3–2) | |
| JSCE [12] | $V_u = 1.45\left[\left(D^2 - d_s^2\right)f_c + d_s^2 f_y\right] - 106.1 \times 10^3$ $73.2 \times 10^3 < \left(D^2 - d_s^2\right)f_c + d_s^2 f_y < 488 \times 10^3$ | (4) | |
| Su et al. [5] | *For* $A_s(\beta\tau_{su} - \tau_{sy}) \le A_c\tau_{cu}$ $Q_u = A_c\tau_{cu} + A_s\tau_{sy}$ | (5–1) | |
| | *For* $A_s(\beta\tau_{su} - \tau_{sy}) > A_c\tau_{cu}$ $Q_u = \beta A_s\tau_{su}$ | (5–2) | |
| Zheng et al. [6] | $V_u = 1.76\alpha_A(A - A_s)f_c + 1.58A_s f_y$ | (6) | |
| He et al. [21] | $V_u = \tau_b A_b + \left(1.06 + 0.07V_f\frac{L_f}{\phi_f}\right)\frac{\pi(D^2-d^2)}{4}f_{cu} + 2.09A_s f_y$ *For normal concrete*: $\tau_b = -0.022f_{cu} + 0.306\sqrt{f_{cu}} - 0.573$ *For UHPC*: $\tau_{bf} = \left(0.04 + 0.04\frac{V_f L_f}{\phi_f}\right)\sqrt{f_{cu}}$ | (7) | |
| Wang et al. [10] | $V_u = 13.972(t_{sc}/D)^{1/2}nD^2\sqrt{f_{ck}} + 3.417b_f L_c + 1.334A_{tr}f_y$ | (8) | |

*Note:* $V_u$= *shear capacity of connector;* $D$ = *Diameter of the hole;* $f_c$ = *Cylindrical concrete strength;* $d_s$ = *Diameter of transverse rebar;* $f_y$ = *Yield strength of reinforcement;* $A_s$= *Area of transverse rebar;* $A_c$ = *Area of concrete dowel;* $\beta$ = *Correction factor;* $\tau_{su}$ = *Ultimate shear strength of rebar;* $\tau_{sy}$ = *Yield shear strength of rebar;* $\tau_{cu}$ = *Nominal shear strength of concrete;* $\alpha_A$ = *Effective shear area ratio of concrete dowel;* $\tau_b$ = *Residual bond strength;* $V_f$ = *Volume content of fibers;* $L_f$ = *Average length of fibers;* $\phi_f$ = *Normalized diameter of fibers;* $f_{cu}$ = *Cubic strength of concrete;* $t_{sc}$ = *Thickness of steel plate;* $n$ = *Number of holes;* $f_{ck}$ = *Compressive concrete strength;* $b_f$ = *Width of steel beam flange;* $L_c$ = *Contact length between steel and concrete.*

**Table 6**
Comparison between Equations for Predicting PBL Ultimate Resistance.

| Specimen code | $V^{Pre.}/V^{Exp.}$ | | | | | | | |
|---|---|---|---|---|---|---|---|---|
| | Hans-Peter [13] Eq. (2) | Vianna et al. [11] Eq. (3–2) | JSCE [12] Eq. (4) | Su et al. [5] Eq. (5–1) | Zheng et al. [6] Eq. (6) | He et al. [21] Eq. (7) | Wang et al. [10] Eq. (8) | Proposed Eq. (16) |
| PR-b1r1d1 | 1.17 | 2.63 | 0.82 | 1.11 | 0.82 | 1.01 | 1.36 | – |
| CR-b1s0p1 | 0.85 | 1.90 | 0.59 | 0.80 | 0.59 | 0.89 | 1.54 | 1.00 |
| Average | 1.01 | 2.27 | 0.71 | 0.96 | 0.71 | 0.95 | 1.45 | 1.00 |

*Note:* $V^{Pre.}$ = *ultimate resistance determined from related equations;* $V^{Exp.}$ = *experimentally obtained ultimate resistance of the connector.*

bearing at the end of the steel plate, which is significantly different from the present PBL specimens' details. Eq. (8) considered the contribution of bonding effects at the steel girder flange/concrete slab contact surface. Eqs. (4) and (6) underestimated the shear capacity of all specimens, while these equations produced very conservative results for the strength of specimen CR-b1s0p1. This is because these two equations were developed based on experimental results from PBL with comparatively lower concrete strength and smaller steel plate/concrete contact area, as compared to the specimens' details evaluated in this study.

The use of Eq. (5–1) (refer to Table 5) resulted in predicting unsafe ultimate resistance for PR-b1r1d1 specimens, while it produced safe results for specimen CR-b1s0p1. It should be noted that the shear resistance computed from this equation consists of two parts: (i) resistance provided by concrete dowel, and (ii) resistance from transverse steel rebar passing through the holes. Furthermore, the bonding contribution at the steel/concrete contact surface is not considered in this expression, which again is different from the push-out test details evaluated in the current study. Another possible reason for the difference between the experimental and predicted results is the relatively lower concrete strength that was used in the push-out tests conducted by Su et al. [5], as compared to the RPC used in presented study.

The ultimate shear strength computed from Eq. (7) was found to have reasonable correlation with the experimental results presented in this paper. It should be noted that this equation was developed using push-out test data for PBL specimens embedded in UHPC, and the contributions of bonding strength at the steel/concrete interface, concrete dowel, and transverse steel rebar were included in the expression. The variations between the predicting and experimental ultimate resistance for CR-b1s0p1 may be ascribed to the influence of RPC shrinkage.

### 4.2. The proposed equation to predict the PBL shear capacity

The aforementioned comparisons between the experimental and analytical results imply that the influence of RPC shrinkage on resistant-bearing capacity of PBL cannot generally be predicted by previous models. A more applicable model is necessary for predicting the shear capacity of PBL in the case of using RPC in CFSCs under natural treatment.

The resistance of PBL encased in CFSC is comprised of: (i) resistance from the interface bond ($V_b$); (ii) resistance from the concrete dowel ($V_c$), and (iii) resistance from the transverse rebar ($V_r$). The ultimate resistance of PBL ($V_u$) is expressed by the following equation:

$$V_u = V_b + V_c + V_r \tag{9}$$

The expressions for the resistance of PBL without considering shrinkage effects are given in reference [7] and are expressed as:

$$V_b = \alpha\sqrt{f_{cu}} \tag{10}$$

$$V_c = 0.4\psi_c A_c f_{cu} \tag{11}$$

$$V_r = 1.15\psi_r A_r f_y \tag{12}$$

where: $\alpha$ = coefficient to be determined by experiment; $f_{cu}$ = the cubic compressive strength of the concrete (MPa); $\psi_c$ = strength enhancement coefficient for concrete dowel under confinement;

$A_c$ = the sectional area of the concrete dowel, and $A_c = \pi\left(D^2 - d_r^2\right)/4$ ($mm^2$), $D$ and $d_r$ are the diameter of the hole and the transverse rebar through the hole, respectively (mm); $\psi_r$ =coefficient for transverse rebar in tension/shear failure mode; $A_r$ = the sectional area of the transverse rebar, and $A_r = \pi d_r^2/4$ (mm2); $f_y$ = the yield strength of transverse rebar (MPa).

Due to the lack of test results for bond strength between steel cell and RPC under natural treatment, the value of $\alpha$ in Eq. (10) is obtained based on the current experimental results. In current work, $f_{cu}$ = 115.5 MPa and the residual resistance of the pure bond specimen CR-b1s0p0 is 350.0 kN. Therefore, the value of $\alpha = 0.06$ can be obtained. The resistance of interface bond can be expressed as:

$$V_b = 0.06\sqrt{f_{cu}} \tag{13}$$

On the other hand, the present experimental results indicated that the mechanical properties of transverse steel rebar passing through the holes were barely influenced by the RPC shrinkage. As such, the $\psi_r = 1.82$ given in reference [7] is taken as the coefficient of the transverse steel rebar in CFSC. Then, the individual contribution of the transverse rebar can be obtained as the following:

$$V_r = 2.09A_r f_y \tag{14}$$

By using Eqs. (13) and (14), the contributions of $V_b$ and $V_r$ to the bearing capacity of specimen CR-b1s0p1 can be calculated, and the value of $\psi_c = 2.91$can also be achieved. The resistance provided by concrete dowel inside the hole can be calculated by:

$$V_c = 1.16A_c f_{cu} \tag{15}$$

Therefore, the ultimate shear capacity of PBL using RPC encased by CFSCs without hot steam curing can be calculated by:

$$V_u = 0.06\sqrt{f_{cu}} + 1.16A_c f_{cu} + 2.09A_r f_y \tag{16}$$

It should be noted that the RPC used in the current tests had design strength of 100 MPa and curing age of 28 days. However, the RPC shrinkage may vary with the material strength and curing age. Thus, it is highly recommended to perform additional tests for the case of RPC with other grade of strength and curing ages. Additionally, it is also recommended that more push-out test data of the PBL embedded in restrained RPC are needed to verify the applicability of the proposed equations.

## 5. Conclusions & recommendations

This study presents a summary of experimental results of push-out specimens consisting of two plug-in type of specimens and eight CFSC type of specimens. Based on experimental load-slip curves and load-strain relationships, structural behavior of steel studs and PBL using RPC and the influence of RPC shrinkage effects on performance of the connectors are analyzed and discussed. The following conclusions can be drawn based on the results of this study:

1. Shrinkage of RPC is very detrimental to the performance of shear connectors encased in CFSC with restrained RPC, however, it has a little influence on the connectors embedded in exposed RPC. Initial cracks at the steel cell/RPC core interface were commonly observed prior to load application. Failure modes of steel studs and transverse rebar of PBL were barely influenced by the RPC shrinkage.
2. Both stiffness and ultimate capacity of connectors encased in steel cells are sensitive to RPC shrinkage. The mechanisms of steel studs and PBL in CFSC were activated at earlier stage due to the premature damage of the steel/concrete bondline caused by the shrinkage. Steel studs and transverse rebars strains at ultimate load are approximately 1200$\mu\varepsilon$, and 2300$\mu\varepsilon$, respectively.
3. Due to the influence of RPC shrinkage, the average bonding strength between steel plate and concrete obtained from the specimens with restrained RPC decreased by 15%, as compared to that of the push-out specimens with exposed RPC. The nominal shear strength of steel studs and PBL embedded in the restrained RPC decreased by 26% and 23%, respectively, as compared to those with exposed RPC.
4. Comparisons between the experimental and equation predicted results imply that the shear capacity of PBL encased in CFSC with RPC cannot generally be predicted by exiting equations. Equations proposed in this study can be potentially used to predict the PBL capacity in CFSC with RPC under natural treatment. However, it is recommended that more push-out experimental data of the PBL using RPC are needed to further verify the applicability of the proposed analytical equations.

## Conflict of interest statement

The authors declare that we have no conflicts of interest to this work. We also declare that we do not have any commercial or associate interest that represents a conflict of interest in connection with the work submitted.

## Acknowledgements

The authors gratefully acknowledge the financial supports from the National Natural Science Foundation of China (Grants No. 51278182 and No. 51408213). The support of the Civil & Environmental Engineering Department at the University of California, Irvine, USA is also acknowledged.

## References

[1] EUROCODE 4. EN 1994-1-1. Design of composite steel and concrete structures Part 1.1 General rules and rules for buildings. Brussels: CEN-European Committee for Standardization, 2005.
[2] L.R.F.D. Aashto, Bridge Design Specifications, 3rd ed., American association of state highway and transportation officials, Washington, D.C, 2004.
[3] Ministry of construction of china GB50017-2014, Code for Design of Steel Structures, China planning press, Beijing, 2014 (In Chinese).
[4] F. Leonhard, W. Andra, H.P. Andra, et al., New, improved bonding means for composite load bearing structures with high fatigue strength, Beton Stahlbetonbau 82 (12) (1987) 325–331.
[5] Q. Su, G. Yang, M.A. Bradford, Bearing capacity of perfobond rib shear connectors in composite girder bridges, J. Bridge Eng. (2016). 06015009.
[6] S. Zheng, Y. Liu, T. Yoda, W. Lin, Parametric study on shear capacity of circular-hole and long-hole perfobond shear connector, J. Constr. Steel Res. 117 (2016) 64–80.
[7] S. He, Z. Fang, A.S. Mosallam, Experimental study on perfobond strip connector in steel-concrete joints of hybrid bridges, J. Constr. Steel Res. 118 (2016) 169–179.
[8] W. Wang, C. Zhao, Q. Li, W. Zhuang, Study on load-slip characteristic curves of perfobond shear connectors in hybrid structures, J. Adv. Concr. Technol. 12 (2014) 413–424.
[9] Q. Zhang, D. Jia, Y. Bao, et al., Analytical study on internal force transfer of perfobond rib shear connector group using a nonlinear spring model, J. Bridge Eng. 22 (10) (2017) 04017081.
[10] X. Wang, B. Zhu, S. Cui, et al., Experimental research on PBL connectors considering the effects of concrete stress state and other connection parameters, J. Bridge Eng. 23 (1) (2018) 04017125.
[11] J.C. Vianna, S.A.L. Andrade, P.C.G.S. Vellasco, et al., Experimental study of Perfobond shear connectors in composite construction, J. Constr. Steel Res. 81 (2013) 62–75.
[12] Standard specifications for steel and composite structures, Japan Society of Civil Engineers (JSCE),Dec, 2009.
[13] Hans-Peter, Economical shear connectors with high fatigue strength. in: International Association for Bridge and Structural Engineering, Isbase Symposium Brussels, 1990, pp. 167–172.
[14] M.X. Xiong, D.X. Xiong, J.Y.R. Liew, Behaviour of steel tubular members infilled with ultra-high strength concrete, J. Constr. Steel Res. 138 (2017) 168–183.

[15] J. Hegger, M. Feldmann, S. Rauscher, et al., High-performance materials in composite construction, Struct. Eng. Int. 4 (2009) 438–446.
[16] C. Zou, Y. Wang, J. Moore, et al., Train-induced field vibration measurements of ground and over-track buildings, Sci. Total Environ. 575C (2017) 1339–1351.
[17] S.B. Medbery, B.M. Shahrooz, Perfobond shear connectors for composite construction, Eng. J. 39 (1) (2002) 2–12.
[18] F.X. Ding, G.A. Yin, H.B. Wang, L.P. Wang, Q. Guo, Static behavior of stud connectors in bi-direction push-off tests, Thin-walled Struct. 120 (2017) 307–318.
[19] Y. Ma, Y. Wang, Creep of high strength concrete filled steel tube columns, Thin-walled Struct. 53 (2012) 91–98.
[20] J. Ji, C. Mi, X. Cao, et al., Design and research on mix proportioning for C55 high performance concrete of hybrid girder cable-stayed bridge, Bridge Constr. 1 (2009) 36–39 (In Chinese).
[21] S. He, Z. Fang, A. Mosallam, Push-out tests for perfobond strip connectors with UHPC grout in the joints of steel-concrete hybrid bridge girders, Eng. Struct. 135 (2017) 177–190.
[22] MCS-EPFL, Recommendation: Ultra-high performance fibre reinforced cement-based composites (UHPFRC) construction material, dimensioning und application, Lausanne, Switzerland, 2016.
[23] S. He, A.S. Mosallam, Z. Fang, C. Zou, W. Feng, J. Su, Experimental study on CFSC encased shear connectors in steel-concrete joints with UHPC grout, Constr. Build. Mater. 173 (2018) 638–649.
[24] Q. Su, W. Wang, H. Luan, et al., Experimental research on bearing mechanism of perfobond rib shear connectors, J. Constr. Steel Res. 95 (2014) 22–31.
[25] J.Y. Kang, J.S. Park, W.T. Jung, et al., Evaluation of the shear strength of perfobond rib connectors in ultra-high performance concrete, Engineering 6 (2014) 989–999.
[26] P. Wirojjanapirom, K. Matsumoto, K. Kono, et al., Experimental study on shear behavior of PBL joint connections for UFC-PC hybrid girder, J. JSCE 2 (2014) 285–298.
[27] GB50917-2013, Code for Design of Steel and Concrete Composite Bridges, 1st ed., China planed press, Beijing, 2013.
[28] C.M. Tam, V.W.Y. Tam, K.M. Ng, Assessing drying shrinkage and water permeability of reactive powder concrete produced in Hong Kong, Constr. Build. Mater. 26 (2012) 79–89.